Monthly Notices
of the
ROYAL ASTRONOMICAL SOCIETY

MNRAS **489,** 4367–4377 (2019)
Advance Access publication 2019 September 7

doi:10.1093/mnras/stz2499

Characteristic radii of the Milky Way globular clusters

Andrés E. Piatti [1,2★] Jeremy J. Webb[3] and Raymond G. Carlberg[3]

[1]*Consejo Nacional de Investigaciones Científicas y Técnicas, Godoy Cruz 2290, C1425FQB Buenos Aires, Argentina*
[2]*Observatorio Astronómico de Córdoba, Laprida 854, 5000 Córdoba, Argentina*
[3]*Department of Astronomy and Astrophysics, University of Toronto, 50 St. George Street, Toronto, ON M5S 3H4, Canada*

Accepted 2019 September 4. Received 2019 September 4; in original form 2019 August 8

ABSTRACT

We report on the extent of the effects of the Milky Way gravitational field in shaping the structural parameters and internal dynamics of its globular cluster population. We make use of a homogeneous, up-to-date data set with kinematics, structural properties, current and initial masses of 156 globular clusters. In general, cluster radii increase as the Milky Way potential weakens; with the core and Jacobi radii being those which increase at the slowest and fastest rate, respectively. We interpret this result as the innermost regions of globular clusters being less sensitive to changes in the tidal forces with the Galactocentric distance. The Milky Way gravitational field also seems to have differentially accelerated the internal dynamical evolution of individual clusters, with those toward the bulge appearing dynamically older. Finally, we find a subpopulation consisting of both compact and extended globular clusters (as defined by their r_h/r_J ratio) beyond 8 kpc that appear to have lost a large fraction of their initial mass lost via disruption. Moreover, we identify a third group with $r_h/r_J > 0.4$, which have lost an even larger fraction of their initial mass by disruption. In both cases the high fraction of mass lost is likely due to their large orbital eccentricities and inclination angles, which lead to them experiencing more tidal shocks at perigalacticon and during disc crossings. Comparing the structural and orbital parameters of individual clusters allows for constraints to be placed on whether or not their evolution was relaxation or tidally dominated.

Key words: globular clusters: general – Galaxy: kinematics and dynamics – Galaxy: structure.

1 INTRODUCTION

It is widely accepted that Milky Way globular clusters have lost most of their masses through three main processes, namely: stellar evolution, two-body relaxation, and tidal heating caused by the Milky Way's gravitational field (Gnedin, Lee & Ostriker 1999; Fall & Zhang 2001; Gieles & Baumgardt 2008; Webb et al. 2013, 2014; Alessandrini et al. 2014; Brockamp et al. 2014). Stellar evolution is most important during the first few hundred million years, while two-body relaxation becomes important as the mass-loss rate due to stellar evolution continues to decrease (Hénon 1961; Heggie & Hut 2003; Gieles, Heggie & Zhao 2011; Shukirgaliyev et al. 2018). Whether or not a cluster is strongly affected by the tidal field depends on its size, mass, and orbit within the Galaxy. Since the strength of the Milky Way tidal field weakens with galactocentric distance, it is expected that mass-loss due to tidal effects follows a similar trend. Hence, the amount of mass lost by very distant globular clusters should be less than those moving in the Milky Way bulge. Furthermore for a given orbit, clusters that are more massive or more compact will have a stronger self-gravity and will be less affected by tidal heating. Such behaviour has been observed within the old globular clusters of the Large Magellanic Cloud, where galaxy's gravitational potential seems to act differently as a function of the cluster distance from the galaxy centre (Piatti & Mackey 2018).

From a purely theoretical approach, the literature is rich with studies on how star clusters are affected by the tidal field of their host galaxy (e.g. Gnedin et al. 1999; Baumgardt & Makino 2003; Heggie & Hut 2003; Lamers et al. 2005; Gieles & Baumgardt 2008; Kruijssen & Mieske 2009; Renaud, Gieles & Boily 2011; Webb et al. 2013, 2014). Most applicable to this study is the work done by Baumgardt & Makino (2003), who performed *N*-body simulations to study how a spherically symmetric external tidal field, in addition to stellar evolution and two-body relaxation, affects the evolution of a star cluster's mass function. They found that mass segregation leads to low-mass stars being preferentially stripped from star clusters, which causes mass functions that initial increase towards the low-mass end to begin decreasing towards the low-mass end (see Webb et al. 2017b, for a direct comparison to observations). From their suite of simulations, Baumgardt & Makino (2003) were also able to generate a relation for estimating a cluster's dissolution time

★ E-mail: andres.piatti@unc.edu.ar

based on its orbit in the galaxy. Expectedly, inner region clusters are expected to dissolve faster than outer region clusters. A secondary dependence exists in the form of cluster's orbital eccentricity, with clusters that have high orbital eccentricities reaching dissolution faster than clusters with low orbital eccentricities but comparable apocenters. It should be noted that the simulations were limited to approximately 10^5 particles. More massive clusters will have less two-body relaxation, $\propto \log N/N$. Tidal heating, which depends on the cluster size, has no dependence on particle mass.

For clusters in non-spherically symmetric tidal fields, tidal heating can also occur in the form of shocks. Spitzer (1958) was the first to study the disruption of clusters due to tidal shocks, and found the amount of mass lost mainly depends on the strength of the shock and the cluster's density within its half-mass radius. Giant molecular clouds (GMCs) are now known to be the dominant source of mass-loss over a cluster's lifetime (Gieles et al. 2006; Lamers & Gieles 2006; Kruijssen et al. 2011; Gieles & Renaud 2016), primarily affecting clusters when they first form and the local GMC encounter rate is high. Focussing on disc shocks in particular, studies have shown that repeated passages through the Galactic disc will accelerate a cluster's dissolution time relative to a cluster orbiting in the plane of the disc (Gnedin & Ostriker 1997; Gieles, Lamers & Portegies Zwart 2007b; D'Onghia et al. 2010; Kruijssen et al. 2011; Webb et al. 2014). Other forms of substructure, including galaxy merger-induced structure (Kruijssen et al. 2012) and dark matter subhaloes (Webb et al. 2019) can also subject a cluster to a tidal shock.

Finally, an additional factor that makes it difficult to estimate a cluster's mass-loss history based on its orbit alone is the fact that a significant fraction of the Galactic cluster population has been accreted (Massari, Koppelman & Helmi 2019). Hence, these clusters have not been on their current orbit for their entire lifetime, and could have lost significantly more (or less) mass than one would predict given their current orbit and structural properties. Luckily the structural properties of accreted clusters are expected to respond to the tidal field of their new host, in this case the Milky Way, very quickly (Miholics, Webb & Sills 2014).

Historically, studies of how Galactic globular clusters have been affected by the Milky Way have been limited by the fact that their orbits were unknown. Hence, conclusions could only be drawn based on their observed properties and their present galactocentric distance. Furthermore, estimates of a cluster's mass and size were taken from a wide range of inhomogeneous studies. As the proper motions of select globular clusters started becoming available, a proper analysis of how individual Galactic globular clusters have been affected by tides was possible (Dinescu, Girard & van Altena 1999; Kruijssen & Mieske 2009; Webb, Harris & Sills 2012; Balbinot & Gieles 2018). In some cases, it was even possible to determine if a cluster's evolution was dominated by two-body relaxation or tidal stripping (Dinescu et al. 1999). Unfortunately, similar to catalogues of globular cluster structural parameters, estimates of cluster orbits were inhomogeneous and typically incomplete. Hence it has been difficult for past studies to identify how strongly a cluster's evolution has been affected by the tidal field of its host galaxy.

With the most recent data release from the European Space Agency's *Gaia* satellite (DR2), the orbit of every Galactic globular cluster is now known (Gaia Collaboration 2018; Baumgardt et al. 2019; Vasiliev 2019). Combining data from *Gaia* DR2 with ground-based line-of-sight velocities and estimates of each cluster's mass and size (Baumgardt & Hilker 2018), Baumgardt et al. (2019) was able to derive the mass lost by each globular cluster since formation by integrating their orbits backwards in time and accounting for dynamical friction.

The Baumgardt et al. (2019) catalogue, which contains cluster positions, space velocities, orbital motion parameters, structural properties, and initial masses of almost all known Milky Way globular clusters (Harris 1996, 2010 December edition) is the most suitable data base for studying the extent that the observed structural properties of clusters have been affected by the Milky Way tidal field. Hence, the purpose of this study is to make use of the Baumgardt et al. (2019) catalogue to analyse how the Milky Way gravitational field affects various observable properties of globular clusters. The estimated fraction of cluster mass lost by disruption serves as a tracer of how strongly a cluster is tidally affected, which can then be compared to several structural and dynamical parameters in order to help constrain a cluster's origin (*in situ* versus accreted), its properties at formation, and whether or not its evolution is dominated by internal or external processes.

The catalogue allows for a homogeneous comparison of a cluster's structural and orbital properties, while also providing an estimate of what each cluster's mass was at formation. This type of study is only possible because Galactic globular clusters are born at the earliest epochs of the Milky Way formation (Kruijssen 2014; Kruijssen et al. 2019) and, consequently, their mass lost due to evolutionary effects is in practice the same (e.g. Lamers et al. 2005). Therefore, it can be expected that any difference between their structural parameters could be due to the difference tidal forces acting on them.

In Section 2, we introduces the data set used in this work. In Section 3, we explore how the estimated fraction of mass lost by each cluster is related to its orbit, several tracers of cluster size, its density profile, dynamical age, and tidal filling factor. Finally, in Section 4 we summarize the main conclusions of this work.

2 DATA HANDLING

To explore how strongly tides have shaped a cluster's evolution, we make use of the Galactic positions (X, Y, Z), space velocities (U, V, W), perigalactic ($R_{\rm peri}$), and apogalactic ($R_{\rm apo}$) distances, and initial ($M_{\rm ini}$) and current ($M_{\rm GC}$) masses of 156 Milky Way globular clusters as derived by Baumgardt et al. (2019). In their study, Baumgardt et al. (2019) estimate cluster positions and velocities using data from *Gaia* DR2. $R_{\rm peri}$ and $R_{\rm apo}$ are then determined by integrating the cluster's orbits assuming the Irrgang et al. (2013) model of the Milky Way. The structural properties of each cluster, mainly their core (r_c) and half-mass (r_h) radius, are taken from Baumgardt & Hilker (2018), who estimate the values by comparing the density profiles of Galactic globular clusters to a large suite of direct N-body star cluster simulations. Since the set of orbital and structural cluster properties have been derived by applying the same methodology, the catalogue represents the largest homogeneous, up-to-date data set of the Milky Way globular cluster system. It is useful to note that Baumgardt et al. (2019) use the Irrgang et al. (2013) model for the Milky Way in order to solve for each cluster's $R_{\rm peri}$ and $R_{\rm apo}$. This model consists of a Plummer sphere bulge, a Miyamoto & Nagai (1975) disc, and a modified Allen & Santillan (1991) dark matter halo. We also performed an independent orbit integration for each cluster using the commonly cited MWPotential2014 Galactic model (Bovy 2015), which consists of a bulge that is represented by a spherical power-law potential, a Miyamoto & Nagai (1975) disc, and a Navarro, Frenk & White (1997) halo. A comparison revealed only minor differences between the orbital parameters of clusters

orbiting in the innermost regions of the Milky Way (which is poorly constrained).

It is important to note that the $M_{\rm ini}$ values in Baumgardt et al. (2019) were obtained by integrating each cluster's orbit backwards in time from their observed positions and space velocities and measured current masses, taking into consideration the dynamical drag force. Using the formalism of Baumgardt & Makino (2003), the authors were able to estimate the mass-loss via tidal stripping. It was additionally assumed that clusters lose half of their $M_{\rm ini}$ due to stellar evolution during their first gigayear (see also de Grijs, Parmentier & Lamers 2005). Baumgardt et al. (2019) iterated over a wide range of $M_{\rm ini}$ values until they were able to recover each cluster's $M_{\rm GC}$, on the basis of a linear mass-loss dependence with time in a spherically symmetric, isothermal galaxy potential over the entire age of each cluster (see also Lamers, Baumgardt & Gieles 2010). One should allow for a dispersion in the fraction of mass lost by disruption of $\sim$ 15–20 per cent due to the uncertainty in the cluster's ages (Helmi et al. 2018; Pfeffer et al. 2018). $M_{\rm ini}$ should also be taken to be a lower limit for several reasons. First, it does not take into account early mass lost by the cluster before it leaves its formation environment and reaches its present-day orbit (Kruijssen 2015). Secondly, interactions with GMCs, which have been shown to be the dominant source of cluster's mass-loss at early times (Gieles et al. 2006; Kruijssen et al. 2011), are also not included in the calculation. Note that accreted clusters were likely not harassed as much by GMCs as *in situ* clusters, while clusters formed in the inner part of the Milky Way likely encountered more GMCs than those formed in the outskirts. Note also that the strength of the tidal field is expected to increase, on average, with cosmic time as the Milky Way grows (Renaud, Agertz & Gieles 2017), and that the presence of the bar (Rossi, Hurley & Ortolani 2018) and spiral arms (Gieles, Athanassoula & Portegies Zwart 2007a) will accelerate mass-loss as well, which is not considered in Baumgardt et al. (2019). Therefore, the estimates of initial mass used in this work are lower limits as many mass-loss mechanisms are not included. In fact, initial mass estimates are perhaps more accurately tracers of the tidal field strength associated with a cluster's current orbit in the present-day potential of the Milky Way.

From the above data set, we computed the semimajor axis of each globular cluster's orbit:

$$a = \frac{R_{\rm peri} + R_{\rm apo}}{2}. \quad (1)$$

The semimajor axis has the advantage of having no time-dependence, as opposed to the cluster's current Galactocentric distance, and is more representative of the mean orbital distance of the globular clusters than $R_{\rm peri}$ or $R_{\rm apo}$. We also computed the orbital eccentricity (ϵ) as

$$\epsilon = \frac{R_{\rm apo} - R_{\rm peri}}{R_{\rm apo} + R_{\rm peri}}, \quad (2)$$

and the values of Jacobi radii from the expression (Chernoff & Weinberg 1990):

$$r_J = \left(\frac{M_{\rm GC}}{3M_{\rm MW}}\right)^{1/3} \times a, \quad (3)$$

where $M_{\rm MW}$ is the Milky Way mass contained within the semimajor axis of cluster's orbit, which is different for each cluster. In order to estimate $M_{\rm MW}$ we used the same Irrgang et al. (2013) Milky Way mass profile that Baumgardt et al. (2019) used to solve the orbit of each cluster. We note that a and e are calculated in a galaxy model that is fitted to the present-day properties of the Milky Way.

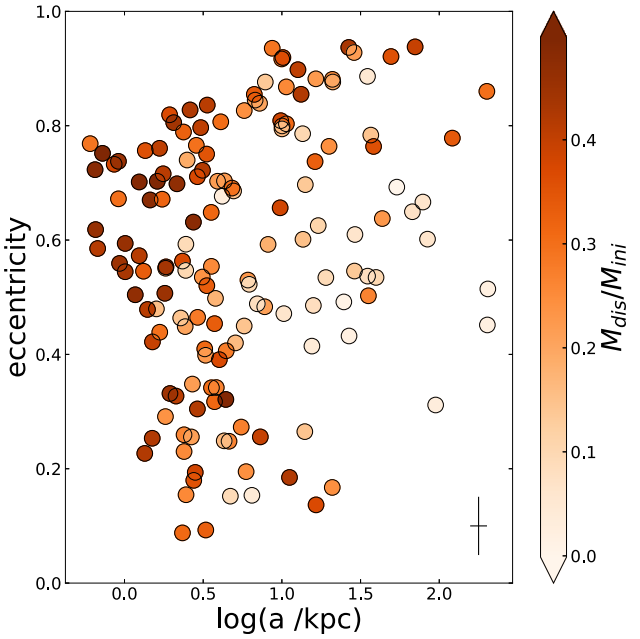

Figure 1. Relationship between the eccentricity, the semimajor axis, and the fraction of disrupted mass for the Baumgardt et al. (2019) globular cluster sample. Typical error bars are indicated.

However, the Milky Way has been grown over time, so that a and e have not been the same over the course of a cluster's lifetime.

Finally, to estimate how much clusters have been disrupted due to relaxation and tidal heating, we split the difference between $M_{\rm ini}$ and $M_{\rm GC}$ up between mass lost via stellar evolution ($M_{\rm ev}$) and mass lost due to disruption ($M_{\rm dis}$):

$$M_{\rm ini} = M_{\rm GC} + M_{\rm ev} + M_{\rm dis}, \quad (4)$$

with $M_{\rm ev} = 0.5 \times M_{\rm ini}$, from which we get

$$M_{\rm dis}/M_{\rm ini} = 1/2 - M_{\rm GC}/M_{\rm ini}. \quad (5)$$

Hence, equation (5) explicitly gives the fraction of cluster mass lost by relaxation and tidal heating as computed (but not tabulated) by Baumgardt et al. (2019). In their study, the authors' only considered the relationship between $M_{\rm GC}$, $M_{\rm ini,}$ and Galactocentric distance (see their fig. 7). In the subsequent analysis we use $M_{\rm dis}/M_{\rm ini}$ as the indicator for tidal field strength.

We estimated the uncertainties of each derived parameter $f(x_1, x_2, \ldots, x_n)$ on the basis of Monte Carlo simulations. We run one thousand calculations of $f(x_1, x_2, \ldots, x_n)$ for each globular cluster with random distributions of each independent variable x_i over the interval $x_i \pm \sigma(x_i)$, for $i = 1, \ldots, n$, where $\sigma(x_i)$ is the error associated to x_i according to Baumgardt et al. (2019). From the resulting distribution of the one thousand generated values, we set the uncertainty of each parameter equal to the range encompassing the central 16 per cent and 84 per cent points.

3 ANALYSIS AND DISCUSSION

We begin our analysis of the Baumgardt & Hilker (2018) and Baumgardt et al. (2019) data with Fig. 1, which depicts the relationship between orbital eccentricity, cluster's semimajor axis, and the fraction of mass lost by disruption. Fig. 1 shows that $M_{\rm dis}/M_{\rm ini}$ is a function of both the semimajor axis and the eccentricity. Likewise, for a given semimajor axis, it is also apparent that the larger the

eccentricity of a cluster's orbit the larger the fraction of mass lost by disruption, as eccentric clusters are brought deeper into the Milky Way's potential well. We note that while this result is simply a byproduct of employing Baumgardt & Makino (2003) to estimate each cluster's initial mass, but it is worth illustrating such a relationship for the actual Milky Way globular cluster system. Highly eccentric clusters are also likely have higher orbital inclinations – consistent with Piatti (2019) – meaning they should dissolve even quicker than estimates by Baumgardt et al. (2019) due to disc shocking (Webb et al. 2014). In fact, Piatti (2019) found that $\sim$ 30 per cent of globular clusters are on orbits with an inclination angle between 20° and 50°. The majority of clusters have even higher inclinations that exceed 50°. Hence, most Galactic globular clusters have undergone several disc crossing compared to those orbiting on more circular orbits in the plane of the disc at a similar distance from the Milky Way centre. Clusters with highly inclined orbits will of course lose more mass (Gnedin et al. 1999; Webb et al. 2014).

Just as interesting are the regions of Fig. 1 where no globular clusters are observed. In general, Milky Way bulge globular clusters ($\log(a/\mathrm{kpc}) < 0.5$) with orbits' eccentricities smaller than ~ 0.5 make up a minor percentage of the total population, as is also the case for outermost ones ($\log(a/\mathrm{kpc}) > 1.5$ with eccentricities smaller than ~ 0.5. This behaviour would seem to be an intrinsic property of the Milky Way globular cluster system, however, likely for different reasons. Bulge clusters are subjected to a very strong tidal field, and therefore expected to lose mass quickly and will likely dissolve within a Hubble time if they are not extremely massive and compact. Hence, the few existing inner region clusters with eccentricities smaller than ~ 0.5 represent the tail end of the initial globular cluster mass and size distributions.

The lack of outer clusters with low eccentricities is consistent with recent work by Piatti (2019), who studied the kinematics properties of the Milky Way globular cluster system and found that outer globular clusters, independent of the direction of their motions (prograde or retrograde orbits), tend to have more radial orbits than those in the disc of the Milky Way and preferentially have large orbital inclination angles. Piatti (2019) also showed that only outer globular clusters that form *in situ* with their host will have radial orbits, accreted globular clusters will have radial orbits regardless of their location in the Milky Way. Finally, by assigning the same probability to an accreted globular cluster to have a prograde or a retrograde orbit, Piatti (2019) found that the accreted to *in situ* globular cluster ratio turns out to be ~ 1. Hence, the lack of outer clusters with low eccentricities is likely due to the fact that most outer halo clusters have been accreted via a past merger. So while the lack of inner region clusters with low eccentricities is due to cluster disruption, the lack of outer region clusters with low eccentricities is likely due to no clusters ever forming there in the first place.

Finally, we also see a region in the top left region of Fig. 1 where no clusters currently exist that extends out to ($\log(a/\mathrm{kpc}) \sim 1.0$. The lack of clusters in this portion of the diagram can again be attributed to cluster disruption, as a small semimajor axis and high orbital eccentricity would bring a cluster deep into the Galaxy's potential well. Hence, any cluster that formed with this orbit would dissolve quickly. A puzzling population exists, however, with intermediate eccentricities ($0.5 < e < 0.8$) and small semimajor axes ($\log(a/\mathrm{kpc}) < 0.5$), which Baumgardt et al. (2019) predict must have been very massive at birth in order to survive a Hubble time. While it is entirely possible that these are simply some of the most massive clusters that have formed in the Milky Way, an alternative explanation would be that these clusters did not always have their present-day orbit. Inward migration is typically due to either dynamical friction

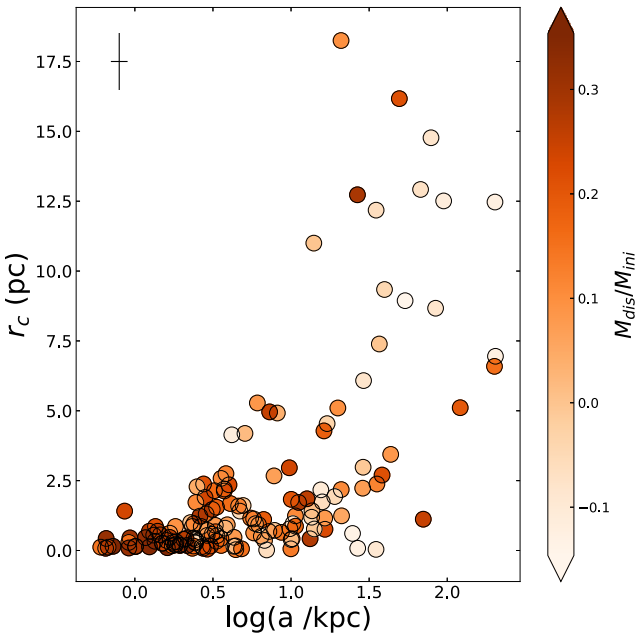

Figure 2. Relationship between the core radius, the semimajor axis, and the fraction of mass lost by disruption for the Baumgardt et al. (2019) globular cluster sample. Typical error bars are indicated.

or an accretion event. In the dynamical friction scenario, which Baumgardt et al. (2019) account for, the clusters were born very massive and have had their orbits decay from a weaker tidal field to a stronger one. Hence, they have not spent their entire lifetime subjected to weak tides. In the accretion scenario, a cluster initially orbit deep in the potential well of a dwarf and is not stripped until its previous host reaches the inner parts of the Milky Way and is near dissolution. In this latter scenario, the cluster still orbits in a strong tidal field for the majority of its life, but while a member of a dwarf galaxy the tidal field may be compressive (Bianchini et al. 2015; Webb, Patel & Vesperini 2017a).

In order for these GCs to migrate inwards, from a weaker tidal field to the strong one they experience at present day, they were likely subject to 1 of 2 mechanisms. Either they were very massive at birth and strongly affected by dynamical friction (which Baumgardt accounts for). Or they were accreted clusters that orbited in the inner regions of a dwarf galaxy. Hence, it was not until their previous host reached the inner Milky Way and was almost completely disrupted that they were accreted.

The different tidal field strengths experienced by globular clusters will also affect their structural parameters, and ultimately their internal dynamical evolutionary stages, with respect to what is expected while evolving in isolation. Figs 2–4 illustrate the relationships between r_c, r_h, and r_J with the semimajor axis and the fraction of mass lost by disruption, respectively. The three figures highlight a general trend, in the sense that any of the derived radii increase as a function of the cluster distance from the Milky Way centre. This outcome was predicted theoretically by Hurley & Mackey (2010) and Bianchini et al. (2015), among others. Globular clusters in weaker tidal fields, like those located in the outermost regions of the Milky Way can expand naturally, whereas those immersed in stronger tidal fields (e.g. the Milky Way bulge) do not. Hence, we see a wider spread in cluster sizes at larger galactocentric distances than in the inner regions of the Galaxy. We also see an absence of significant outliers in these figures due to accreted clusters, as

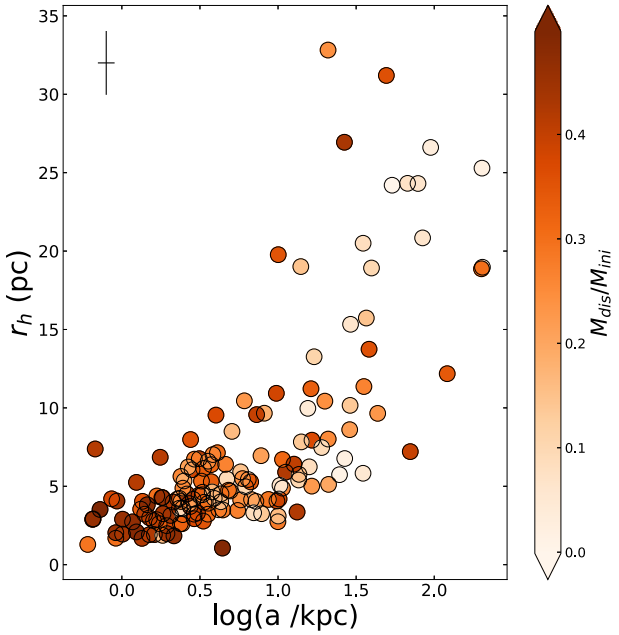

Figure 3. Relationship between the half-mass radius, the semimajor axis, and the fraction of mass lost by disruption for the Baumgardt et al. (2019) globular cluster sample. Typical error bar is indicated.

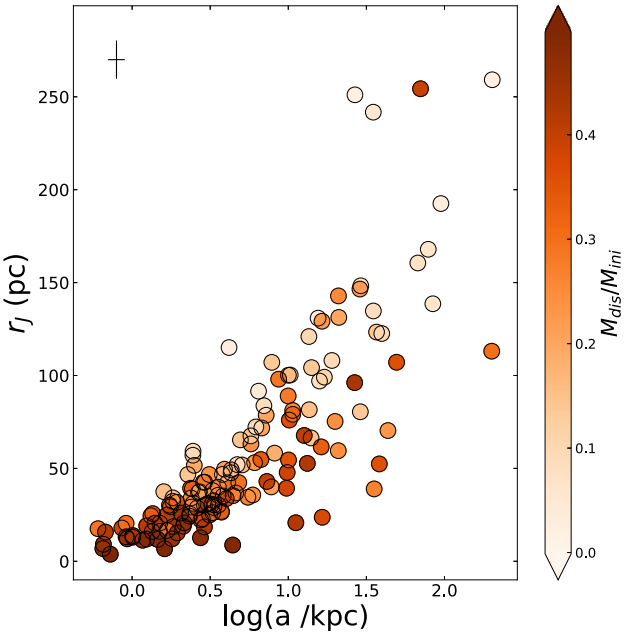

Figure 4. Relationship between the Jacobi radius, the semimajor axis, and the fraction of mass lost by disruption for the Baumgardt et al. (2019) globular cluster sample. Typical error bars are indicated.

Miholics et al. (2014) have shown the size of an accreted cluster will quickly respond to the tidal field of the Milky Way.

When comparing Figs 2–4, some more subtle differences do arise. More specifically, r_c, r_h, and r_J all increase with semimajor axis at different paces and the spread in radius at a given log(a/kpc) is also different. Indeed, r_c is the radius that increases the slowest with log(a/kpc), while r_J shows the fastest growth. This behaviour is particularly noticeable for globular clusters inside a circle of 10 kpc

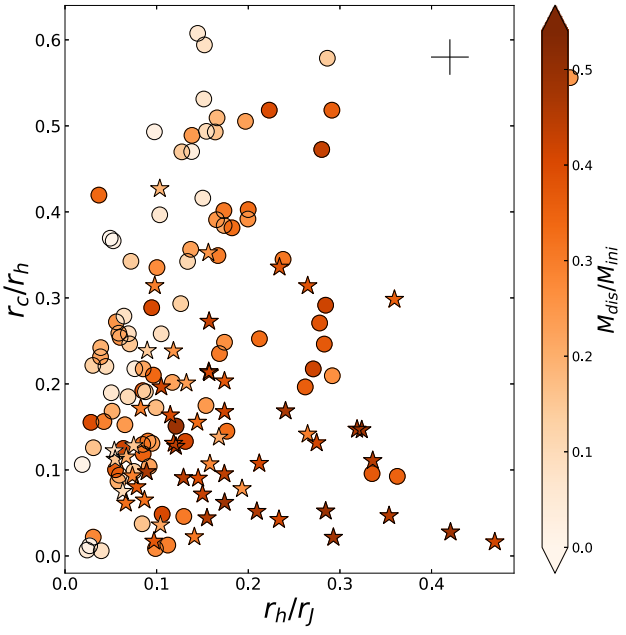

Figure 5. Relationship between r_c, r_h, and r_J radii. Typical error bars are indicated. Filled stars and circles represent clusters located inside and outside the bulge volume (log(a/kpc) $= 3$), respectively.

(log(a/kpc) < 1.0). For instance, the mean r_c, r_h, and r_J values at log(a/kpc) $= 1$ are 2, 5, and 10 times those at log(a/kpc) $= -0.3$, respectively. This result expectedly indicates that the innermost regions of globular clusters are less sensitive to external changes in the Milky Way gravitational field. Similarly, with the cluster's inner regions being less affected by tides than its outer regions, we observe a larger spread in r_c than we do for r_h and r_J. Since outer region clusters are less affected by the tidal field, with most likely not having expanded to the point of becoming tidally filling (Hénon 1961; Alexander & Gieles 2013), the rate of increase in r_c, r_h, and r_J is primarily the result of the initial size and mass distribution of globular clusters and the combined effects of stellar evolution and two-body relaxation. Similar trends are detected in the ancient globular clusters of the Large Magellanic Cloud (Piatti & Mackey 2018), whose sizes, the Elson, Fall & Freeman (1987) power-law slopes at large radii (γ, Mackey & Gilmore 2004), ratios of the cluster radius to Jacobi radius, and the inverse of the concentration parameter c increase with the deprojected galactocentric distance. Similar trends are also seen in giant elliptical galaxies (Harris 2009; Webb et al. 2016).

Heggie & Hut (2003) have described the internal dynamics evolution of a star cluster as seen in the r_c/r_h versus r_h/r_J plane. As a star cluster expands to the point of being tidally filling, it experiences violent relaxation in its core region followed by two-body relaxation, mass segregation, and finally core-collapse. These processes result in clusters evolving from having high r_c/r_h and low r_h/r_J to low r_c/r_h and high r_h/r_J. We examined such a diagnostic diagram for our 156 globular cluster sample and connect the observed trends with those of Figs 1–4 by using the same colour scale given by the range of $M_{\rm dis}/M_{\rm ini}$. We find that the Milky Way tidal field has had a role in shaping the internal dynamical evolution of clusters as well.

Fig. 5 shows that core-collapse globular clusters are mainly Milky Way bulge objects (log(a/kpc) $\lesssim 0.5$). They occupy the region delimited by $r_c/r_h \lesssim 0.2$ and $r_h/r_J \gtrsim 0.30$. Likewise, the

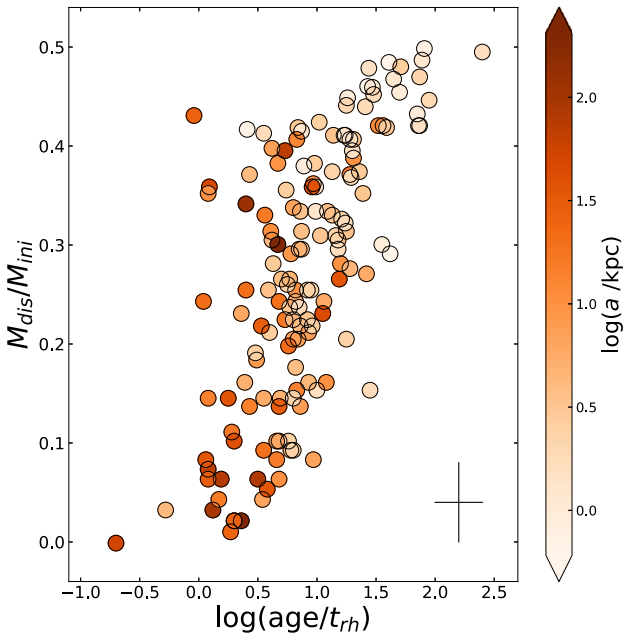

Figure 6. Globular cluster fraction of mass disrupted by tidal effects as a function of the age/t_{rh} ratio. Typical error bars are indicated.

least dynamically evolved globular clusters would appear to be the outermost ones ($r_c/r_h \gtrsim 0.45$). Although globular clusters have been born with different masses and sizes, and hence they should stay at different internal dynamic stages even if they were evolved in isolation, the fact that those at a more advanced dynamical stage are the ones located in inner Milky Way regions reveals that the Milky Way potential well has differentially accelerated their internal dynamical evolution. Having lost a large fraction of their initial masses and having their sizes tidally limited will minimize an inner region cluster's relaxation time, allowing it to evolve quickly compared to outer region clusters which lose little mass and can expand to large sizes. Note, for instance, that globular clusters that have lost more than 45 per cent of their masses by disruption are mostly bulge globular clusters at an advanced evolutionary stage, and conversely, those with $M_{\rm dis}/M_{\rm ini} \lesssim 0.10$ – located in the outermost Milky Way regions – are relatively less evolved globular clusters. Some degeneracy exists, of course, as some clusters were likely to have been more with short initial relaxation times and reached the core-collapse phase simply through rapid relaxation. The mostly likely candidates for having their evolution be internally (relaxation) driven as opposed to through interactions with the tidal field are cluster with low r_c/r_h that are not predicted to have lost much mass via tidal stripping (lighter points).

Further evidence of such a differential acceleration of the globular cluster internal dynamics evolution is depicted in Fig. 6, where we plot the fraction of mass lost by disruption as a function of the ratio between each cluster's age and its half-mass relaxation time (age/t_{rh}). Value for t_{rh} is taken from Baumgardt et al. (2019), where t_{rh} is calculated using the formalism of Baumgardt & Hilker (2018). Globular cluster ages were assumed to be $12^{-1.5}_{-2.0}$ Gyr (Kruijssen et al. 2019). As can be seen in Fig. 6, globular clusters with $M_{\rm dis}/M_{\rm ini} \gtrsim 0.45$ ($\log(a\,/\,{\rm kpc}) \lesssim 0.5$) have apparently lived many more median relaxation times than their more remote counterparts ($M_{\rm dis}/M_{\rm ini} \lesssim 0.10$, which corresponds to $\log(a/{\rm kpc}) \gtrsim 1.5$). The small or negligible amount of mass lost by disruption of the outermost globular clusters lead us to conclude that most of the amount of mass lost during their lifetimes should have been by relaxation. Even for a given dynamical age, there is a clear spread in $M_{\rm dis}/M_{\rm ini}$ that can be attributed to cluster orbit (as traced by each cluster's semimajor axis in the colour bar). This spread helps separate between whether or not a cluster's dynamical age is the result of its formation properties or tidal interactions.

Fig. 6 also shows that globular clusters that have lost between 15 and 40 per cent of their masses by disruption have similar dynamical ages. These globular clusters mostly populate the Milky Way disc ($0.5 \lesssim \log(a/{\rm kpc}) \lesssim 1.4$), so that the range of mass fraction lost is primarily linked to the globular cluster's distance from the Galactic centre. We checked whether globular clusters with highly eccentric orbits could have affected their age/t_{rh} ratios because of their many disc crossings, and found that they do not differentiate from those with smaller eccentricities. Indeed, Fig. 1 shows that globular clusters with eccentricities > 0.8 have lost between ~ 15 and 45 per cent of their masses by disruption, a $M_{\rm dis}/M_{\rm ini}$ range where $\log({\rm age}/t_{rh})$ is nearly constant (0.75 ± 0.25, see Fig. 6).

Baumgardt et al. (2010) investigated the r_h/r_J ratio of Galactic globular clusters as given by the Milky Way potential and found that the r_h/r_J ratio is a good discriminator between globular clusters that are compact and extended at birth. This ratio has also long been the criteria for determining whether a cluster is tidally filling or not, with clusters that have $r_h/r_J > 0.145$ considered to be tidally filling (Hénon 1965). Baumgardt et al. (2010) found that for Galactocentric distances larger than 8 kpc, r_h/r_J ratios smaller than 0.05 correspond to initially compact objects, while r_h/r_J ratios between 0.1 and 0.3 point to globular clusters intrinsically larger, and not because of expansion in a weaker tidal field. Both groups of globular clusters would have an *in situ* origin. To further expand their study on compact and extended clusters, in the left-hand panel of Fig. 7 we reproduce the Baumgardt et al. (2010) fig. 2 comparing r_h/r_J to each cluster's semimajor axis for our enlarged globular cluster sample. In order to make Fig. 7 as informative as possible, we included some other cluster orbital motion parameters, namely, the orbit eccentricity and inclination; the latter split in arbitrary bins. In both panels, symbol sizes are proportional to each cluster's orbital eccentricity and symbol shapes are related to their orbital inclinations (i). For comparison purposes, we also show in the right-hand panel r_h/r_J versus each cluster's perigalactic distance, where in this case r_J is calculated at perigalacticon.

For reference purposes, we include Table A1 in the Appendix containing all the relevant information used in making Fig. 7. Table A1 serves as a useful source for identifying clusters that are tidally filling or underfilling both on average and near pericentre. Clusters that are tidally underfilling at pericentre have likely had their evolution governed by two-body relaxation, while clusters that are on average tidally filling have likely had their evolution strongly shaped by the tidal field. For all other clusters, a combination of relaxation and tidal interactions have played a role in their evolution and it is not necessarily the case that one mechanism is more dominant over the other.

The left-hand panel of Fig. 7 shows that, in general, the smaller the distance from the Milky Way centre the larger the r_h/r_J ratio. This would seem to be a consequence of inner region clusters easily expanding to the point of being tidally filling due to stellar evolution and two-body relaxation. Hence, they have experienced a significant amount of mass-loss due to disruption, primarily of low-mass stars that have segregated outwards, leaving the surviving globular clusters with their more massive members (Baumgardt & Makino 2003; Khalisi, Amaro-Seoane & Spurzem 2007). Therefore, as

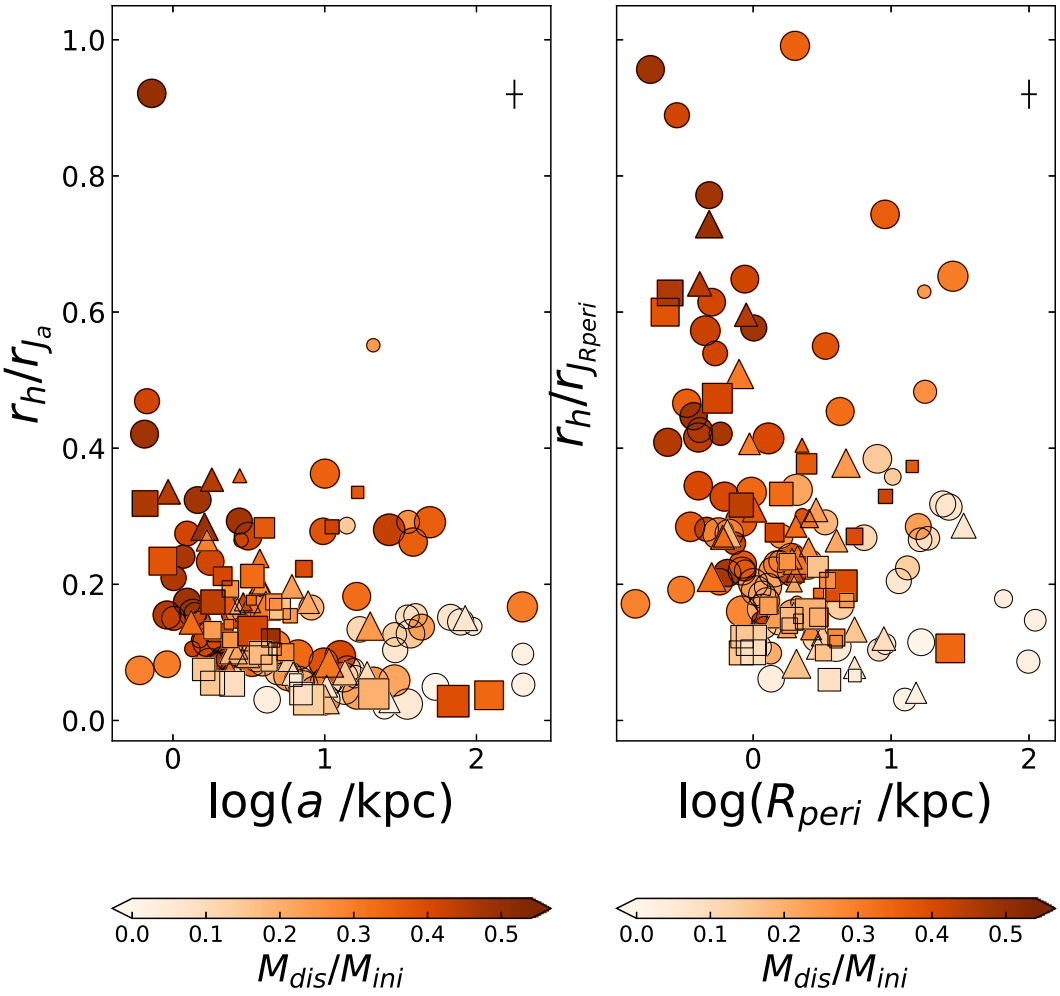

Figure 7. *Left-hand panel:* r_h/r_J compared to each cluster's semimajor axis, where r_J is calculated at cluster's semimajor distance. *Right-hand panel:* r_h/r_J compared to each cluster's pericentre, where r_J is calculated at the cluster's perigalactic distance. Typical error bars are indicated. According to Baumgardt et al. (2010), globular clusters located at Galactocentric distances > 8 kpc and below $r_h/r_J = 0.1$ or $0.1 < r_h/r_J < 0.3$ are genuine compact and extended objects at birth, respectively. Symbol sizes are proportional to the orbit eccentricities ($0 < \epsilon < 1$), while triangles, squares, and circles correspond to orbit inclinations (i) between $i \leq 30°$, $30° < i \leq 60°$ and $i > 60°$, respectively.

expected, their $M_{\rm dis}/M_{\rm ini}$ ratios are amongst the largest in the data set. In the inner regions of the galaxy there is significant scatter about this general trend, as first pointed out by Baumgardt et al. (2010), which is likely a remnant of the range of initial masses and sizes clusters can have at birth.

In the outer regions of the galaxy (beyond $\sim$ 8 kpc), tidally underfilling clusters continue to follow the general trend of r_h/r_J with galactocentric distance down to a mean value of 0.05. Given the relatively weak external tidal field that these clusters are subject to, their evolution is almost entirely dominated by internal processes. However, beyond 8 kpc there also exists a population of tidally filling clusters. Previous work by Baumgardt et al. (2010) also recognized that outer region clusters with log(a/kpc) > 0.9 could be separated into tidally underfilling ($r_h/r_J < 0.05$) and filling ($0.1 < r_h/r_J < 0.3$) populations. We further separate the filling clusters into two additional subpopulations, with $r_h/r_J \sim 0.2$ (barely tidally filling) and $r_h/r_J >= 0.3$ (tidally overfilling), based on an apparent gap in the r_h/r_J distribution of outer region clusters. Given the relatively weak tidal field the clusters experience, tidally filling outer region clusters are likely to either be accreted, have high eccentricities, or formed quite extended.

Independent of semimajor axis, we identify a potential third group of globular clusters with $0.4 < r_h/r_J < 1.0$. Clusters in this group also have highly eccentric and inclined orbits, such that they are subject to strong tidal shocks at pericentre and during disc passages. Given that these four clusters are severely tidally overfilling, they should be in the process of dissolving.

The right-hand panel of Fig. 7 is also of interest, as it indicates that almost every cluster is tidally filling at perigalacticon. Hence, while the few that are not tidally filling at perigalacticon can be considered to have had their evolution be relaxation dominated, the majority of clusters are affected by the tidal field to some degree. Clusters that are tidally filling at their semimajor axis (left-hand panel) are most likely to have their evolution be tidally dominated.

4 CONCLUSIONS

We have analysed the relationships between the Milky Way globular clusters structural parameters, their internal dynamical stages, and the fraction of mass lost by tidal effects (disruption). There has long been a general understanding that the Milky Way gravitational field

has played a strong role in the globular cluster mass-loss process along their lifetimes.

We made use of publicly available positions, space velocity components, orbital motion parameters, core, half-mass and tidal radii, relaxation times, current and initial masses of 156 Milky Way globular clusters, from which we addressed the issue about at what extent the Milky Way potential well has acted in shaping their present-day sizes and dynamical age. As suggested by previous theoretical results, we started by analysing the relationship between the fraction of mass lost by disruption, the globular cluster distance to the Milky Way centre and the eccentricity of their orbits. We find an absence of cluster with short semimajor axes and either low or high orbital eccentricities, likely due to the fact that any clusters born in this regime would reach dissolution fairly quickly. Although a puzzling population of clusters with intermediate eccentricities and short semimajor axes is observed, also with relatively high orbital inclinations. There is also a lack of outer region clusters with low orbital eccentricities, likely due to outer region clusters primarily being accreted clusters that have orbits that are comparable to the radial orbit in which their progenitor host galaxy fell in on.

The core, half-mass, and Jacobi radii of Galactic clusters show different rates of increase with Galactocentric distance, in the sense that the core radii increases slower than the half-mass radii, which in turn increases at a slower pace than Jacobi radii. This outcome would seem to suggest that the inner most regions of globular clusters are less sensitive to changes in the Milky Way potential with the Galactocentric distance. On the contrary, their outermost regions would appear more vulnerable.

From the different fractions of mass lost by disruption of each cluster, we found that the Milky Way gravitational field has differentially accelerated the internal dynamical evolution of its globular clusters. Having been stripped of a large fraction of their initial mass, and having their sizes tidally limited, inner region clusters will have shorter relaxation times than outer region clusters. Hence, globular clusters located in the bulge would seem to be at a more advanced internal dynamical evolutionary stage, approaching to or at the core-collapse stage, while more distant globular clusters have lived many fewer median relaxation times than their innermost counterparts.

Finally, we confirmed the existence of two intrinsically different size globular cluster groups as identified by Baumgardt et al. (2010) at large Galactocentric distances. That is to say we find globular clusters can primarily be split into groups with $r_h/r_J \sim 0.05$ and 0.20 that have lost a very small fraction of their initial mass. However, we point out that interspersed within both groups are clusters that have lost a large percentage of their masses by disruption. Hence, it is more difficult to distinguish between clusters that are compact and extended at birth from their r_h/r_J ratio alone. There is a third group of objects with $r_h/r_J > 0.4$ which have lost even more mass due to tidal effects. In both cases, clusters that have lost a large portion of their initial mass have highly eccentric orbits with large inclination angles, which leads to them experiencing more tidal shocks at perigalacticon and while crossing the disc. Hence, they have lost an additional fraction of mass over what their semimajor axis alone implies. These clusters are, most likely, clusters that have been accreted by the Milky Way and have had their structural properties respond to their new host.

ACKNOWLEDGEMENTS

We thank the referee, Florent Renaud, for a timely and constructive report to improve the manuscript. We thank Henny J.G.L.M. Lamers and Mark Gieles for their reading through an earlier version of this manuscript and timely comments and Holger Baumgardt for providing us with his globular cluster data base.

REFERENCES

Alessandrini E., Lanzoni B., Miocchi P., Ciotti L., Ferraro F. R., 2014, ApJ, 795, 169
Alexander P. E. R., Gieles M., 2013, MNRAS, 432, L1
Allen C., Santillan A., 1991, Rev. Mex. Astron. Astrofis., 22, 255
Balbinot E., Gieles M., 2018, MNRAS, 474, 2479
Baumgardt H., Hilker M., 2018, MNRAS, 478, 1520
Baumgardt H., Makino J., 2003, MNRAS, 340, 227
Baumgardt H., Parmentier G., Gieles M., Vesperini E., 2010, MNRAS, 401, 1832
Baumgardt H., Hilker M., Sollima A., Bellini A., 2019, MNRAS, 482, 5138
Bianchini P., Renaud F., Gieles M., Varri A. L., 2015, MNRAS, 447, L40
Bovy J., 2015, ApJS, 216, 29
Brockamp M., Küpper A. H. W., Thies I., Baumgardt H., Kroupa P., 2014, MNRAS, 441, 150
Chernoff D. F., Weinberg M. D., 1990, ApJ, 351, 121
D'Onghia E., Springel V., Hernquist L., Keres D., 2010, ApJ, 709, 1138
de Grijs R., Parmentier G., Lamers H. J. G. L. M., 2005, MNRAS, 364, 1054
Dinescu D. I., Girard T. M., van Altena W. F., 1999, AJ, 117, 1792
Elson R. A. W., Fall S. M., Freeman K. C., 1987, ApJ, 323, 54
Fall S. M., Zhang Q., 2001, ApJ, 561, 751
Gaia Collaboration, 2018, A&A, 616, A12
Gieles M., Baumgardt H., 2008, MNRAS, 389, L28
Gieles M., Renaud F., 2016, MNRAS, 463, L103
Gieles M., Portegies Zwart S. F., Baumgardt H., Athanassoula E., Lamers H. J. G. L. M., Sipior M., Leenaarts J., 2006, MNRAS, 371, 793
Gieles M., Athanassoula E., Portegies Zwart S. F., 2007a, MNRAS, 376, 809
Gieles M., Lamers H. J. G. L. M., Portegies Zwart S. F., 2007b, ApJ, 668, 268
Gieles M., Heggie D. C., Zhao H., 2011, MNRAS, 413, 2509
Gnedin O. Y., Ostriker J. P., 1997, ApJ, 474, 223
Gnedin O. Y., Lee H. M., Ostriker J. P., 1999, ApJ, 522, 935
Harris W. E., 1996, AJ, 112, 1487
Harris W. E., 2009, ApJ, 699, 254
Heggie D., Hut P., 2003, The Gravitational Million-Body Problem: A Multidisciplinary Approach to Star Cluster Dynamics. Cambridge Univ. Press , Cambridge
Helmi A., Babusiaux C., Koppelman H. H., Massari D., Veljanoski J., Brown A. G. A., 2018, Nature, 563, 85
Hénon M., 1961, Ann. Astrophys., 24, 369
Hénon M., 1965, Ann. Astrophys., 28, 62
Hurley J. R., Mackey A. D., 2010, MNRAS, 408, 2353
Irrgang A., Wilcox B., Tucker E., Schiefelbein L., 2013, A&A, 549, A137
Khalisi E., Amaro-Seoane P., Spurzem R., 2007, MNRAS, 374, 703
Kruijssen J. M. D., 2014, Class. Quantum Gravity, 31, 244006
Kruijssen J. M. D., 2015, MNRAS, 454, 1658
Kruijssen J. M. D., Mieske S., 2009, A&A, 500, 785
Kruijssen J. M. D., Pelupessy F. I., Lamers H. J. G. L. M., Portegies Zwart S. F., Icke V., 2011, MNRAS, 414, 1339
Kruijssen J. M. D., Pelupessy F. I., Lamers H. J. G. L. M., Portegies Zwart S. F., Bastian N., Icke V., 2012, MNRAS, 421, 1927
Kruijssen J. M. D., Pfeffer J. L., Reina-Campos M., Crain R. A., Bastian N., 2019, MNRAS, 486, 3180
Lamers H. J. G. L. M., Gieles M., 2006, A&A, 455, L17
Lamers H. J. G. L. M., Gieles M., Bastian N., Baumgardt H., Kharchenko N. V., Portegies Zwart S., 2005, A&A, 441, 117
Lamers H. J. G. L. M., Baumgardt H., Gieles M., 2010, MNRAS, 409, 305
Mackey A. D., Gilmore G. F., 2004, MNRAS, 352, 153
Massari D., Koppelman H. H., Helmi A., 2019, preprint (arXiv:1906.08271)
Miholics M., Webb J. J., Sills A., 2014, MNRAS, 445, 2872

Miyamoto M., Nagai R., 1975, PASJ, 27, 533
Navarro J. F., Frenk C. S., White S. D. M., 1997, ApJ, 490, 493
Pfeffer J., Kruijssen J. M. D., Crain R. A., Bastian N., 2018, MNRAS, 475, 4309
Piatti A. E., 2019, ApJ, 882, 98
Piatti A. E., Mackey A. D., 2018, MNRAS,
Renaud F., Gieles M., Boily C. M., 2011, MNRAS, 418, 759
Renaud F., Agertz O., Gieles M., 2017, MNRAS, 465, 3622
Rossi L. J., Hurley J. R., Ortolani S., 2018, MNRAS, 480, 1912
Shukirgaliyev B., Parmentier G., Just A., Berczik P., 2018, ApJ, 863, 171
Spitzer Lyman J., 1958, ApJ, 127, 17
Vasiliev E., 2019, MNRAS, 484, 2832
Webb J. J., Harris W. E., Sills A., 2012, ApJ, 759, L39
Webb J. J., Harris W. E., Sills A., Hurley J. R., 2013, ApJ, 764, 124
Webb J. J., Sills A., Harris W. E., Hurley J. R., 2014, MNRAS, 445, 1048
Webb J. J., Sills A., Harris W. E., Gómez M., Paolillo M., Woodley K. A., Puzia T. H., 2016, MNRAS, 460, 2129
Webb J. J., Patel S. S., Vesperini E., 2017a, MNRAS, 468, 92
Webb J. J., Vesperini E., Dalessandro E., Beccari G., Ferraro F. R., Lanzoni B., 2017b, MNRAS, 471, 3845
Webb J. J., Bovy J., Carlberg R. G., Gieles M., 2019, MNRAS, 488, 5748

APPENDIX A: MILKY WAY GLOBULAR CLUSTERS' PARAMETERS

Table A1. Milky Way globular clusters' parameters used to build Fig. 7.

ID	a (kpc)	$R_{\rm peri}$ (pc)	rh/r_{J_a}	$rh/r_{J_{\rm Rperi}}$	ϵ	i (deg)
NGC 104	6.45 ± 0.01	5.46 ± 0.01	0.06	0.07	0.15 ± 0.00	27.78 ± 0.80
NGC 288	8.17 ± 0.28	3.33 ± 0.49	0.17	0.29	0.59 ± 0.05	124.77 ± 1.83
NGC 362	6.76 ± 0.23	1.05 ± 0.21	0.06	0.19	0.84 ± 0.03	85.40 ± 3.63
Whiting1	35.46 ± 4.48	17.64 ± 4.08	0.29	0.48	0.50 ± 0.10	71.76 ± 4.24
NGC 1261	10.67 ± 0.85	1.41 ± 0.36	0.06	0.22	0.87 ± 0.03	110.52 ± 9.87
Pal1	16.49 ± 0.89	14.23 ± 0.91	0.34	0.37	0.14 ± 0.05	14.45 ± 5.28
AM1	203.59 ± 89.87	98.84 ± 39.38	0.05	0.09	0.51 ± 0.26	110.20 ± 41.25
Eridanus	84.24 ± 14.67	33.56 ± 23.03	0.15	0.29	0.60 ± 0.22	46.82 ± 28.63
Pal2	20.95 ± 1.83	2.49 ± 1.80	0.06	0.23	0.88 ± 0.08	144.05 ± 35.09
NGC 1851	9.98 ± 0.11	0.83 ± 0.05	0.03	0.16	0.92 ± 0.00	93.82 ± 1.71
NGC 1904	10.15 ± 0.59	0.82 ± 0.33	0.06	0.29	0.92 ± 0.03	81.65 ± 5.22
NGC 2298	9.84 ± 0.73	1.88 ± 0.79	0.08	0.24	0.81 ± 0.07	121.07 ± 5.94
NGC 2419	53.74 ± 4.06	16.52 ± 2.68	0.05	0.11	0.69 ± 0.05	60.48 ± 6.22
Pyxis	78.74 ± 15.69	26.26 ± 8.98	0.14	0.31	0.67 ± 0.11	102.92 ± 3.94
NGC 2808	7.85 ± 0.06	0.97 ± 0.02	0.03	0.12	0.88 ± 0.00	13.05 ± 20.09
E3	11.18 ± 1.40	9.11 ± 0.44	0.28	0.33	0.18 ± 0.10	28.91 ± 9.65
Pal3	94.87 ± 25.51	65.31 ± 23.15	0.14	0.18	0.31 ± 0.23	71.59 ± 15.90
NGC 3201	15.85 ± 0.61	8.15 ± 0.09	0.06	0.10	0.49 ± 0.02	152.31 ± 2.73
Pal4	67.51 ± 14.82	23.66 ± 22.78	0.15	0.32	0.65 ± 0.28	67.95 ± 55.01
Crater	202.23 ± 89.57	110.92 ± 47.45	0.10	0.15	0.45 ± 0.29	109.03 ± 60.62
NGC 4147	13.24 ± 1.32	1.92 ± 0.77	0.06	0.22	0.86 ± 0.06	83.73 ± 2.13
NGC 4372	5.07 ± 0.08	2.94 ± 0.14	0.16	0.23	0.42 ± 0.02	28.59 ± 4.93
Rup106	19.94 ± 2.04	4.71 ± 0.67	0.14	0.38	0.76 ± 0.04	46.00 ± 8.58
NGC 4590	19.03 ± 1.44	8.86 ± 0.42	0.07	0.12	0.53 ± 0.04	41.04 ± 8.30
NGC 4833	4.09 ± 0.16	0.79 ± 0.12	0.17	0.51	0.81 ± 0.03	44.23 ± 9.88
NGC 5024	15.52 ± 0.92	9.09 ± 0.16	0.08	0.11	0.41 ± 0.04	74.80 ± 1.44
NGC 5053	13.99 ± 0.68	10.28 ± 0.09	0.29	0.36	0.26 ± 0.04	76.11 ± 1.15
NGC 5139	4.18 ± 0.03	1.35 ± 0.04	0.03	0.06	0.68 ± 0.01	138.06 ± 0.89
NGC 5272	10.29 ± 0.21	5.44 ± 0.09	0.05	0.08	0.47 ± 0.01	56.37 ± 2.46
NGC 5286	7.21 ± 0.45	1.16 ± 0.24	0.05	0.16	0.84 ± 0.03	125.18 ± 18.04
AM4	200.68 ± 92.69	28.07 ± 2.24	0.17	0.65	0.86 ± 0.07	83.67 ± 10.52
NGC 5466	36.74 ± 13.50	7.95 ± 2.63	0.13	0.38	0.78 ± 0.10	107.25 ± 2.20
NGC 5634	14.09 ± 1.86	4.27 ± 2.30	0.08	0.17	0.70 ± 0.14	64.17 ± 2.87
NGC 5694	35.01 ± 3.92	3.98 ± 0.95	0.02	0.11	0.89 ± 0.03	124.95 ± 8.69
IC4499	17.02 ± 1.83	6.38 ± 1.24	0.13	0.27	0.63 ± 0.07	112.45 ± 1.86
NGC 5824	26.72 ± 5.64	15.17 ± 5.45	0.03	0.04	0.43 ± 0.18	57.22 ± 2.76
Pal5	20.90 ± 4.11	17.40 ± 6.04	0.55	0.63	0.17 ± 0.20	65.13 ± 2.14
NGC 5897	6.09 ± 0.87	2.86 ± 1.05	0.20	0.31	0.53 ± 0.14	59.50 ± 12.47
NGC 5904	13.55 ± 0.53	2.90 ± 0.05	0.04	0.12	0.79 ± 0.01	74.09 ± 0.66
NGC 5927	4.70 ± 0.09	3.99 ± 0.02	0.10	0.12	0.15 ± 0.02	9.13 ± 20.45
NGC 5946	3.33 ± 0.46	0.83 ± 0.43	0.09	0.22	0.75 ± 0.12	77.17 ± 1.91
NGC 5986	2.86 ± 0.28	0.67 ± 0.31	0.10	0.27	0.77 ± 0.10	60.88 ± 11.67
FSR1716	3.74 ± 0.31	2.55 ± 0.42	0.24	0.30	0.32 ± 0.09	32.33 ± 11.77
Pal14	49.36 ± 4.57	3.90 ± 1.90	0.29	1.70	0.92 ± 0.04	75.06 ± 193.30
Lynga7	3.24 ± 0.26	1.91 ± 0.39	0.17	0.24	0.41 ± 0.09	36.06 ± 9.71
NGC 6093	1.93 ± 0.14	0.35 ± 0.10	0.08	0.28	0.82 ± 0.05	97.02 ± 2.65

Table A1 – *continued*

ID	a (kpc)	$R_{\rm peri}$ (pc)	rh/r_{J_a}	$rh/r_{J_{\rm Rperi}}$	ϵ	i (deg)
NGC 6121	3.36 ± 0.06	0.55 ± 0.08	0.13	0.47	0.84 ± 0.02	4.96 ± 7.66
NGC 6101	29.13 ± 5.14	11.37 ± 1.07	0.10	0.20	0.61 ± 0.07	143.36 ± 8.63
NGC 6144	2.82 ± 0.30	2.27 ± 0.31	0.26	0.30	0.19 ± 0.10	116.71 ± 3.09
NGC 6139	2.43 ± 0.36	1.34 ± 0.45	0.07	0.10	0.45 ± 0.15	62.30 ± 5.09
Ter3	2.76 ± 0.23	2.26 ± 0.11	0.36	0.40	0.18 ± 0.07	42.91 ± 6.72
NGC 6171	2.34 ± 0.09	1.02 ± 0.15	0.17	0.31	0.56 ± 0.05	49.25 ± 6.55
ESO452-SC11	1.62 ± 0.19	0.48 ± 0.18	0.28	0.73	0.70 ± 0.10	48.30 ± 1.71
NGC 6205	4.94 ± 0.08	1.55 ± 0.04	0.07	0.15	0.69 ± 0.01	105.00 ± 0.74
NGC 6229	16.44 ± 1.73	1.94 ± 1.49	0.04	0.16	0.88 ± 0.09	73.83 ± 16.27
NGC 6218	3.57 ± 0.06	2.35 ± 0.10	0.13	0.17	0.34 ± 0.02	36.79 ± 4.40
FSR1735	3.13 ± 0.44	0.87 ± 0.27	0.27	0.65	0.72 ± 0.08	67.41 ± 5.27
NGC 6235	13.62 ± 9.74	5.43 ± 1.53	0.07	0.13	0.60 ± 0.30	39.53 ± 2.06
NGC 6254	3.28 ± 0.05	1.97 ± 0.04	0.12	0.16	0.40 ± 0.01	42.78 ± 1.89
NGC 6256	2.34 ± 0.32	2.13 ± 0.47	0.14	0.15	0.09 ± 0.14	18.53 ± 8.09
Pal15	26.61 ± 2.86	1.68 ± 0.92	0.28	1.75	0.94 ± 0.03	110.49 ± 39.89
NGC 6266	1.59 ± 0.06	0.83 ± 0.08	0.07	0.12	0.48 ± 0.04	29.05 ± 6.51
NGC 6273	2.28 ± 0.14	1.22 ± 0.11	0.09	0.14	0.46 ± 0.05	99.61 ± 12.71
NGC 6284	4.32 ± 0.62	1.28 ± 0.39	0.09	0.20	0.70 ± 0.09	90.47 ± 0.62
NGC 6287	3.56 ± 0.80	1.25 ± 0.26	0.09	0.18	0.65 ± 0.10	95.88 ± 0.50
NGC 6293	1.76 ± 0.46	0.50 ± 0.18	0.23	0.61	0.72 ± 0.11	130.42 ± 54.17
NGC 6304	2.39 ± 0.24	1.77 ± 0.23	0.19	0.23	0.26 ± 0.09	19.66 ± 31.83
NGC 6316	3.12 ± 0.89	1.45 ± 0.87	0.09	0.15	0.54 ± 0.24	34.75 ± 2.86
NGC 6341	5.76 ± 0.12	1.00 ± 0.09	0.07	0.20	0.83 ± 0.01	83.79 ± 1.45
NGC 6325	1.35 ± 0.34	1.04 ± 0.13	0.11	0.13	0.23 ± 0.20	106.50 ± 1.38
NGC 6333	3.90 ± 0.39	1.16 ± 0.15	0.09	0.19	0.70 ± 0.04	64.73 ± 3.63
NGC 6342	1.50 ± 0.25	1.12 ± 0.34	0.12	0.15	0.25 ± 0.17	62.88 ± 3.56
NGC 6356	5.76 ± 1.16	3.17 ± 1.58	0.09	0.13	0.45 ± 0.21	43.18 ± 2.20
NGC 6355	1.50 ± 0.46	0.87 ± 0.24	0.15	0.22	0.42 ± 0.20	103.08 ± 0.84
NGC 6352	3.28 ± 0.30	2.98 ± 0.25	0.18	0.19	0.09 ± 0.09	13.33 ± 13.74
IC1257	10.03 ± 1.37	2.01 ± 0.72	0.36	0.99	0.80 ± 0.07	158.42 ± 31.57
Ter2	0.65 ± 0.23	0.18 ± 0.06	0.42	0.96	0.72 ± 0.13	158.97 ± 26.47
NGC 6366	3.74 ± 0.10	2.04 ± 0.11	0.20	0.29	0.45 ± 0.02	34.87 ± 4.76
Ter4	0.93 ± 0.29	0.41 ± 0.22	0.34	0.64	0.56 ± 0.22	46.85 ± 2.07
HP1	1.24 ± 0.33	0.53 ± 0.23	0.27	0.54	0.57 ± 0.18	87.68 ± 0.54
NGC 6362	3.83 ± 0.05	2.52 ± 0.09	0.20	0.25	0.34 ± 0.02	44.18 ± 3.07
Lil1	0.61 ± 0.16	0.14 ± 0.11	0.07	0.17	0.77 ± 0.17	162.65 ± 31.56
NGC 6380	1.35 ± 0.37	0.33 ± 0.10	0.16	0.47	0.76 ± 0.09	157.67 ± 14.22
Ter1	0.86 ± 0.31	0.23 ± 0.17	0.23	0.60	0.73 ± 0.19	13.39 ± 11.30
Ton2	2.90 ± 0.44	2.02 ± 0.31	0.17	0.22	0.30 ± 0.12	35.55 ± 3.74
NGC 6388	2.45 ± 0.05	1.11 ± 0.02	0.06	0.11	0.55 ± 0.01	154.64 ± 5.03
NGC 6402	2.50 ± 0.13	0.65 ± 0.17	0.10	0.28	0.74 ± 0.06	46.95 ± 5.07
NGC 6401	1.32 ± 0.38	0.60 ± 0.41	0.14	0.27	0.55 ± 0.26	51.33 ± 6.60
NGC 6397	4.43 ± 0.02	2.63 ± 0.03	0.10	0.13	0.41 ± 0.00	47.06 ± 0.42
Pal6	2.06 ± 0.37	0.40 ± 0.10	0.12	0.42	0.81 ± 0.06	82.84 ± 0.78
NGC 6426	121.07 ± 83.20	26.84 ± 5.46	0.04	0.11	0.78 ± 0.16	20.93 ± 4.24
Djor1	70.25 ± 71.73	4.36 ± 1.76	0.03	0.20	0.94 ± 0.07	6.00 ± 17.61
Ter5	1.82 ± 0.31	0.82 ± 0.32	0.05	0.10	0.55 ± 0.15	12.69 ± 74.47
NGC 6440	0.91 ± 0.19	0.30 ± 0.12	0.08	0.19	0.67 ± 0.13	113.79 ± 2.79
NGC 6441	2.45 ± 0.08	1.00 ± 0.08	0.05	0.10	0.59 ± 0.03	20.82 ± 8.51
Ter6	0.92 ± 0.28	0.24 ± 0.09	0.15	0.41	0.74 ± 0.12	157.28 ± 21.98
NGC 6453	2.91 ± 0.84	1.56 ± 0.90	0.16	0.23	0.46 ± 0.26	78.02 ± 1.02
UKS1	0.65 ± 0.19	0.25 ± 0.22	0.32	0.63	0.62 ± 0.29	11.86 ± 37.46
NGC 6496	7.78 ± 3.87	4.02 ± 0.94	0.17	0.26	0.48 ± 0.27	30.99 ± 5.88
Ter9	0.73 ± 0.24	0.18 ± 0.09	0.92	2.29	0.75 ± 0.14	69.96 ± 2.58
Djor2	1.83 ± 0.46	0.82 ± 0.37	0.17	0.32	0.55 ± 0.19	11.51 ± 6.50
NGC 6517	2.37 ± 0.37	0.50 ± 0.15	0.07	0.21	0.79 ± 0.07	58.10 ± 5.92
NGC 6522	0.68 ± 0.17	0.28 ± 0.20	0.47	0.89	0.59 ± 0.25	71.88 ± 123.80
Ter10	1.68 ± 0.29	0.94 ± 0.23	0.26	0.41	0.44 ± 0.13	58.94 ± 0.74
NGC 6535	2.74 ± 0.16	1.01 ± 0.23	0.29	0.58	0.63 ± 0.07	161.39 ± 27.30
NGC 6528	1.01 ± 0.44	0.41 ± 0.10	0.21	0.43	0.59 ± 0.19	65.60 ± 1.95
NGC 6539	2.66 ± 0.13	1.98 ± 0.16	0.17	0.20	0.26 ± 0.05	56.14 ± 5.48
NGC 6540	2.12 ± 0.31	1.43 ± 0.37	0.21	0.28	0.33 ± 0.14	22.44 ± 1.48
NGC 6544	3.05 ± 0.19	0.62 ± 0.20	0.11	0.33	0.80 ± 0.06	66.51 ± 1.67

Table A1 – *continued*

ID	a (kpc)	$R_{\rm peri}$ (pc)	rh/r_{J_a}	$rh/r_{J_{\rm Rperi}}$	ϵ	i (deg)
NGC 6541	2.70 ± 0.14	1.76 ± 0.21	0.10	0.14	0.35 ± 0.06	46.22 ± 4.45
ESO280-SC06	9.75 ± 1.45	3.35 ± 1.77	0.28	0.55	0.66 ± 0.16	61.52 ± 3.56
NGC 6553	1.82 ± 0.15	1.29 ± 0.22	0.13	0.17	0.29 ± 0.09	13.70 ± 50.10
2MASS-GC02	1.46 ± 0.27	0.48 ± 0.22	0.32	0.77	0.67 ± 0.14	170.20 ± 78.55
NGC 6558	1.17 ± 0.42	0.58 ± 0.10	0.24	0.42	0.50 ± 0.19	62.45 ± 22.78
IC1276	4.61 ± 0.31	3.47 ± 0.12	0.17	0.21	0.25 ± 0.05	10.88 ± 43.39
Ter12	4.41 ± 0.26	2.99 ± 0.26	0.12	0.15	0.32 ± 0.05	18.98 ± 1.82
NGC 6569	2.39 ± 0.63	1.84 ± 0.92	0.12	0.14	0.23 ± 0.27	26.98 ± 47.90
BH261	1.94 ± 0.36	1.30 ± 0.55	0.13	0.17	0.33 ± 0.20	34.28 ± 0.83
NGC 6584	10.68 ± 3.70	2.10 ± 1.08	0.08	0.24	0.80 ± 0.11	52.19 ± 3.19
NGC 6624	1.01 ± 0.09	0.46 ± 0.14	0.15	0.28	0.54 ± 0.11	68.41 ± 7.54
NGC 6626	1.74 ± 0.13	0.57 ± 0.10	0.09	0.20	0.67 ± 0.05	60.27 ± 3.62
NGC 6638	1.67 ± 0.45	0.40 ± 0.13	0.11	0.34	0.76 ± 0.09	77.99 ± 3.32
NGC 6637	1.40 ± 0.32	0.73 ± 0.54	0.16	0.26	0.48 ± 0.29	74.26 ± 1.27
NGC 6642	1.24 ± 0.16	0.37 ± 0.15	0.17	0.45	0.70 ± 0.11	62.26 ± 8.94
NGC 6652	2.15 ± 0.54	0.65 ± 0.49	0.09	0.22	0.70 ± 0.20	74.62 ± 0.91
NGC 6656	6.20 ± 0.03	2.96 ± 0.05	0.07	0.11	0.52 ± 0.01	33.66 ± 1.91
Pal8	4.01 ± 0.74	2.44 ± 1.11	0.28	0.38	0.39 ± 0.21	22.17 ± 5.51
NGC 6681	2.91 ± 0.15	0.84 ± 0.08	0.10	0.23	0.71 ± 0.03	91.13 ± 3.71
NGC 6712	2.61 ± 0.07	0.45 ± 0.10	0.16	0.57	0.83 ± 0.04	83.31 ± 6.76
NGC 6715	24.76 ± 1.08	12.58 ± 0.47	0.02	0.03	0.49 ± 0.03	83.60 ± 0.55
NGC 6717	1.81 ± 0.15	0.89 ± 0.17	0.35	0.60	0.51 ± 0.08	34.60 ± 6.62
NGC 6723	2.46 ± 0.08	2.08 ± 0.14	0.16	0.17	0.15 ± 0.03	86.46 ± 9.56
NGC 6749	3.34 ± 0.19	1.60 ± 0.28	0.21	0.33	0.52 ± 0.07	3.59 ± 122.04
NGC 6752	4.30 ± 0.04	3.23 ± 0.08	0.08	0.10	0.25 ± 0.01	25.96 ± 2.85
NGC 6760	3.79 ± 0.11	1.90 ± 0.09	0.10	0.15	0.50 ± 0.02	6.80 ± 75.96
NGC 6779	6.68 ± 0.43	0.97 ± 0.38	0.10	0.34	0.85 ± 0.05	106.58 ± 8.68
Ter7	28.93 ± 9.38	13.14 ± 2.68	0.13	0.22	0.55 ± 0.16	84.81 ± 0.64
Pal10	5.52 ± 0.21	4.01 ± 0.31	0.10	0.12	0.27 ± 0.04	7.62 ± 40.80
Arp2	39.67 ± 10.04	18.46 ± 3.05	0.15	0.27	0.53 ± 0.13	76.93 ± 1.25
NGC 6809	3.57 ± 0.08	1.59 ± 0.02	0.17	0.27	0.55 ± 0.01	67.31 ± 1.06
Ter8	35.05 ± 10.66	16.23 ± 3.06	0.15	0.27	0.54 ± 0.15	82.98 ± 0.80
Pal11	7.30 ± 1.21	5.43 ± 2.07	0.22	0.27	0.26 ± 0.19	26.14 ± 11.54
NGC 6838	5.93 ± 0.03	4.77 ± 0.06	0.15	0.18	0.19 ± 0.01	11.87 ± 11.19
NGC 6864	10.02 ± 1.50	2.06 ± 1.15	0.03	0.08	0.79 ± 0.11	49.76 ± 8.30
NGC 6934	21.06 ± 5.32	2.60 ± 1.12	0.04	0.16	0.88 ± 0.06	23.41 ± 46.62
NGC 6981	12.65 ± 2.29	1.29 ± 0.74	0.09	0.41	0.90 ± 0.06	67.90 ± 35.70
NGC 7006	28.76 ± 2.84	2.07 ± 0.94	0.06	0.34	0.93 ± 0.03	135.42 ± 28.56
NGC 7078	6.98 ± 0.05	3.57 ± 0.06	0.04	0.06	0.49 ± 0.01	28.59 ± 1.69
NGC 7089	8.68 ± 0.30	0.56 ± 0.10	0.04	0.27	0.94 ± 0.01	84.10 ± 28.49
NGC 7099	4.82 ± 0.25	1.49 ± 0.05	0.11	0.23	0.69 ± 0.02	118.50 ± 6.29
Pal12	43.46 ± 18.94	15.75 ± 1.92	0.14	0.28	0.64 ± 0.16	67.35 ± 3.08
Pal13	38.26 ± 5.50	9.04 ± 1.74	0.26	0.74	0.76 ± 0.05	112.26 ± 6.36
NGC 7492	16.25 ± 1.88	4.27 ± 2.29	0.18	0.45	0.74 ± 0.12	91.70 ± 1.20

This paper has been typeset from a TEX/LATEX file prepared by the author.